Current Science International
ISSN 2077-4435

Volume : 04 | Issue : 01 | Jan.-Mar.|2015
Pages: 01-09

Current Transport Mechanisms of Au/n-$GeSe_4$/p-Si/Al Heterojunctions

M.H. Ali

Physics Department, Faculty of Science, Ain Shams University, Abbassia, 11556 Cairo, Egypt.

ABSTRACT

In this report, Au/n-$GeSe_4$/p-Si/Al heterojunction is studied. The I-V characteristics were studied in the temperature range 308-373 K. The junction parameters were investigated. This study showed that the thermionic emission (TE) mechanism is the operating mechanism at low forward voltage (V≤0.3 V). Study of the ideality factor and the barrier heights with temperature indicated deviation from the TE theory. This was explained by the spatially inhomogeneous barriers with Gaussian distribution of barrier heights. The Gaussian parameters were determined. The capacitance-voltage (C-V) of Au/n-$GeSe_4$/p-Si/Al heterojunction was also investigated. The built-in voltage, the capacitance at zero bias and the depletion width were calculated to be 0.574 V, 2.33×10^{-10} F, and 0.42 μm, respectively.

Key words: Heterojunction, $GeSe_4$, Si, Transport conduction mechanisms.

Introduction

Non-crystalline chalcogens and chalcogenides (S, Se, and Te based compounds) were extensively studied for several decades because of their interesting scientific importance and technological applications (Borrisova, 1981; Kokorina, 1996; Hamakawa, 1981; Popescu, 2000 and references cited therein). They are used in optical communications, microelectronics, integrated optics, optical imaging and recording. Several research works have been published on the heterojunctions between amourphous and single-crystalline semiconductors (Capasso, 1987; El-Nahass *et al.*, 2012, 2014; Aksoy *et al.*, 2012). Several microelectronics devices have been fabricated using chalcogenide semiconductors e.g. rectifiers (Anderson, 1962) and solar cells (Hor *et al.*, 1983; Tucci *et al.*, 2007).

Chalcogenide amorphous materials based on Ge-Se glasses are promising candidate for optoelectronic applications (Sedeek *et al.*, 2008; Lee *et al.*, 2015). These materials, due to their photoinduced phenomena, are important for the application as optical memories and photoresistors (Tikhomirov *et al.*, 2003; Russo *et al.*, 2005). Therefore, due to their promising applications, Ge-Se glasses have been intensively studied in last decade. Ge-Se amorphous materials have promising properties such as wide glass range, high stability and large transmission range (Pan *et al.*, 2013). Compositions of Ge-Se glasses play an important role in the structure and properties of these glasses.

Several authors reported the optical properties of thermally evaporated $GeSe_4$ thin films (Thakur *et al.*, 2007; Hafiz *et al.* 2007). While, Pan *et al.*, (2009) investigated the annealing effects on the structure and optical properties of $GeSe_2$ and $GeSe_4$ thin films prepared by pulsed laser deposition technique. Troles *et al.*, (2009) fabricated $GeSe_4$ glass fiber with low optical losses in the mid–IR.

The aim of this paper is to report on the preparation of Au/n-$GeSe_4$/p-Si/Al heterojunction and to study the transport conduction mechanisms in forward and reverse directions. By analyzing the current-voltage-temperature relations as well as the capacitance-voltage measurements, the junction parameters were reported.

Experimental:

Semiconductor p-Si wafer have (100) orientation, 400 μm thickness and 1-10 Ω.cm resistivity was used in this study. Si wafers were etched using the etching solution of HF: HNO_3:CH_3COOH in ratio 1:6:1 as reported earlier (El-Nahass *et al.*, 2014). High-purity aluminum (5N) was thermally deposited on the backside of Si wafer as a back ohmic electrode. $GeSe_4$thin films of thickness 160 nm were deposited on the top of Si wafer. Then, $GeSe_4$ thin films were coated by Au-mesh. Thermal evaporation technique was used to deposit $GeSe_4$ films, Al and Au electrodes using Edward evaporation unit (E306A), under vacuum of 1.33×10^{-4} Pa. A quartz thickness monitor (Edward FTM6) monitored the film thickness. X-ray diffraction study was performed using Phillips X′Pert diffractometer. The chemical composition analysis was studied using energy dispersive X-ray (EDX) spectroscopy attached to scanning electron microscope (JEOL 5400).

The current–voltage (I-V) characteristics measurements were measured at temperature range 308–373 K using high impedance programmable electrometer (Keithley 2635A). Measurements were performed using dark

Corresponding Author: M.H. Ali, Physics Department, Faculty of Science, Ain Shams University, Abbassia, 11556 Cairo, Egypt.
E-mail: mhali_55@hotmail.com

oven. The capacitance-voltage (C-V) characteristics were measured at 1 MHz at room temperature, using CV-410 meter (Solid State Measurement, Inc., Pittsburgh).

Results and Discussion

Fig. 1 shows the X-ray diffraction pattern of as deposited $GeSe_4$ thin films. Figure shows the amorphous nature of the thin film. Inset of the figure shows the (EDX) of the films. The analysis of the constituent elements were 19.23, 80.77 at % for Ge and Se, respectively. This confirms that the composition of the deposited films were as the expected values.

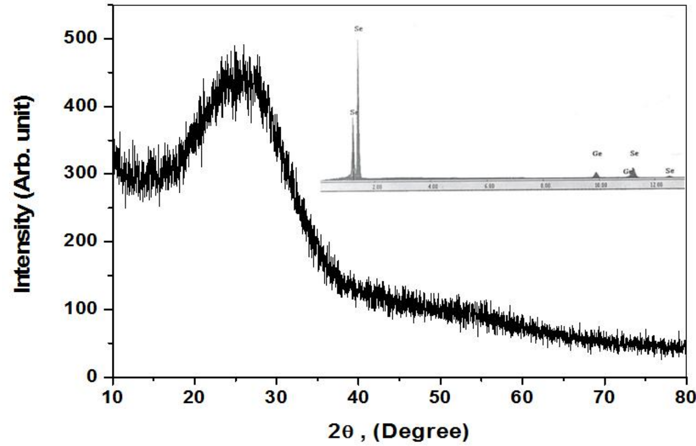

Fig. 1: XRD pattern of $GeSe_4$ thin films, the inset figure is the EDX of the film.

Study of the I-V characteristics gives important information about the junction parameters. Rectification ratio (RR), Series resistance (R_s), shunt resistance (R_{sh}), diode ideality factor (n) and zero barrier height (Φ_B) and the type of the predominant conduction mechanisms are important parameters. Fig. 2 shows the I-V characteristics of Au/n-$GeSe_4$/p-Si/Al heterojunction at temperature range 308-373 K. It is clear that the curves exhibit diode-like behavior. The current increases with increasing temperature at the same applied voltage.

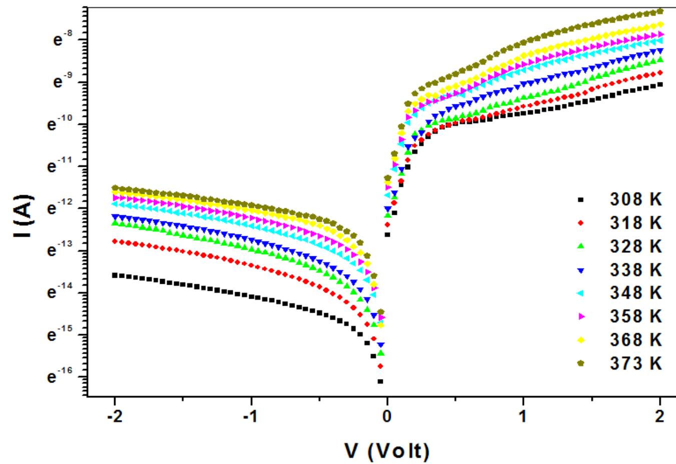

Fig. 2: Dark *I-V* characteristics for Au/n-$GeSe_4$/p-Si/Al heterojunction at different temperatures.

The rectification ratio (RR) of the Au/n-$GeSe_4$/p-Si/Al heterojunction is the ratio of the forward to the reverse currents at certain constant applied voltage. The RR is calculated at ± 1V and the calculated values were given in Table 1.

The series resistances (R_s), at different temperatures, were calculated from the slopes of the linear parts in I-V curves at high forward biasing. The calculated values are tabulated in Table 1. It is clear that as the temperature increases, the series resistance decreases. This may be responsible for the decrease of the ideality factor with increasing temperature. To confirm the obtained values of R_s, the resistance of the junction (R_j) is calculated from studying R_j versus V. At high forward bias, the junction resistance approaches a constant value,

which is the series resistance, R_s. However, at high reverse bias, the junction resistance is also constant, which is the shunt resistance R_{sh}. The obtained values of R_s and R_{sh} are given in table 1.

Table 1: The temperature dependence of RR, R_{Sh}, R_j, R_S, Φ_B and n for Au/n-$GeSe_4$/p-Si/Al heterojunction.

Temp., K	R.R	R_{Sh}, MΩ	R_j, kΩ	R_S, kΩ I-V	Φ_B, eV I-V	Φ_B, eV Norde	n
308	77.11	1.588	17.45	15.313	0.466	0.458	3.57
318	43.66	7.067	13.14	4.250	0.476	0.482	3.45
328	36.33	4.630	9.711	3.508	0.487	0.491	3.30
338	40.58	3.864	7.667	3.496	0.498	0.502	3.10
348	40.26	2.905	6.057	2.747	0.505	0.501	3.02
358	38.62	2.471	5.197	2.433	0.516	0.516	2.88
368	39.46	2.174	4.159	2.409	0.528	0.526	2.78
373	47.64	1.989	3.027	1.473	0.533	0.544	2.62

To study the transport conduction mechanism, semi-logarithmic plots of the forward I-V characteristics at different temperature are shown in Fig. 3. It is clear that, the I-V curves can be divided into two regions. The first region is at low forward bias (0≤V≤0.25 V), and the second region at higher forward bias (V≥0.3V) which is ohmic. At low bias voltage, the forward current is an exponential function of the applied voltage. The slope of the straight lines is found to be inversely proportional with the increase of temperature. Therefore, it is concluded that thermionic emission (TE) is the predominant conduction mechanism at that voltage range.

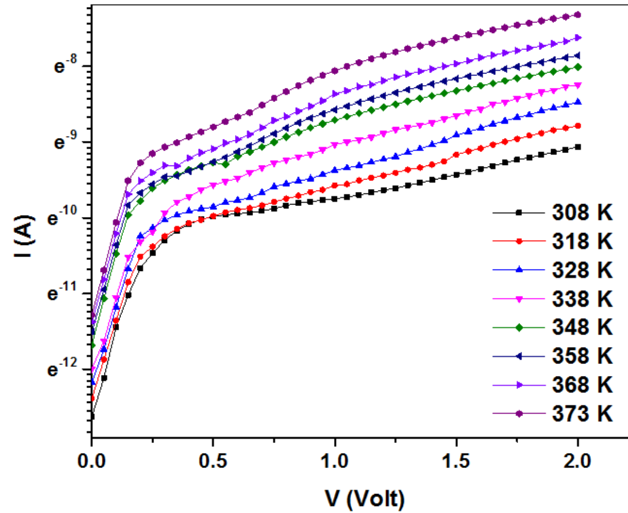

Fig. 3: Variation of ln I_f versus forward bias for Au/n-$GeSe_4$/p-Si/Al heterojunction at different temperatures.

The I-V characteristics for a junction based on the thermionic emission (TE) model are given by (Sze, 1981)

$$I = I_o\left[\exp\left(\frac{q(V-IR_s)}{nkT}\right)-1\right] \quad (1)$$

where I_o is the saturation current, q is the electronic charge, V is the applied voltage, IR_s term is the voltage drop across the series resistance of the junction, n is the ideality factor k is the Boltzman constant and T is the absolute temperature. The saturation current can be obtained from the extrapolation of the forward-bias current at a zero bias voltage and it is given by

$$I_o = AA^*T^2 \exp\left(-\frac{q\Phi_B}{kT}\right) \quad (2)$$

where A is the effective area, A^* is the Richardson constant (32 $Acm^{-2}K^{-2}$ for p-Si) (El-Nahass *et al*, 2014; Sze, 1981; Cetinkara *et al.*, 2003) and Φ_B is the zero-bias barrier height which can be calculated from the relation

$$\Phi_B = \frac{kT}{q} \ln\left(\frac{AA^*T^2}{I_o}\right) \quad (3)$$

While, the ideality factor (n) is calculated from the slope of the linear portion of the forward-bias of I-V characteristics (Fig. 3) using the relation

$$n = \frac{q}{kT}\left(\frac{dV}{d\ln I}\right) \quad (4)$$

The experimental calculation of Φ_B and n were determined using equation (3) and (4) and are given in Table 1.

To confirm that the thermionic emission is the predominant transport conduction mechanism, the plot between $ln(\frac{I_o}{T^2})$ versus 1000/T is depicted in Fig. 4. It is clear from the figure that the relation is straight line confirming that the thermionic emission is the operating conduction mechanism. The slope of the straight line is used to calculate the barrier height and it was found to be 0.151 eV.

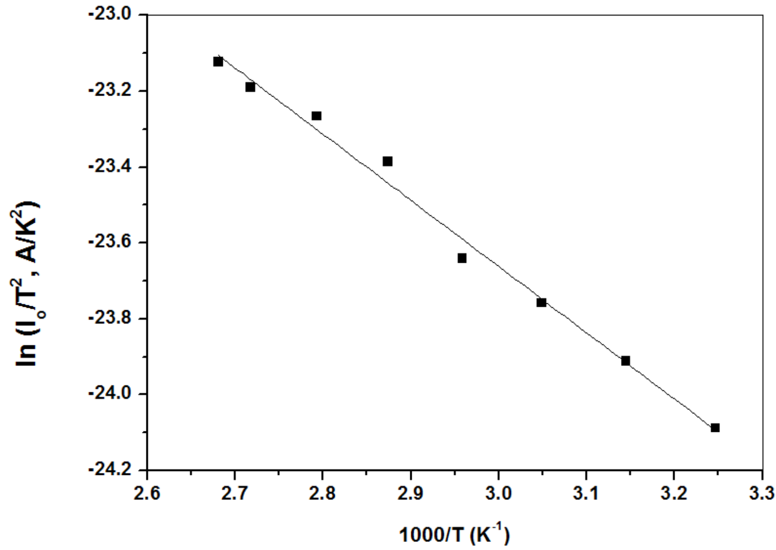

Fig. 4: Richardson plot of ln *(I_o/T^2)* versus reciprocal temperature of Au/n-$GeSe_4$/p-Si/Al heterojunction.

The values of reverse saturation current I_o (obtained from Fig. 3) is related to the temperature according to the relation,

$$I_o = I_s \exp\left(\frac{-E_a}{kT}\right) \quad (5)$$

where I_s is the pre-exponential factor and E_a is the activation energy. Fig. 5 shows the plot of *ln* I_o versus *1000/T*. The activation energy was calculated from the slope of the linear relation and found to be 0.21 eV. This value is in agreement with literature (Aksoy *et al.*, 2012; Zhang *et al.*, 2006).

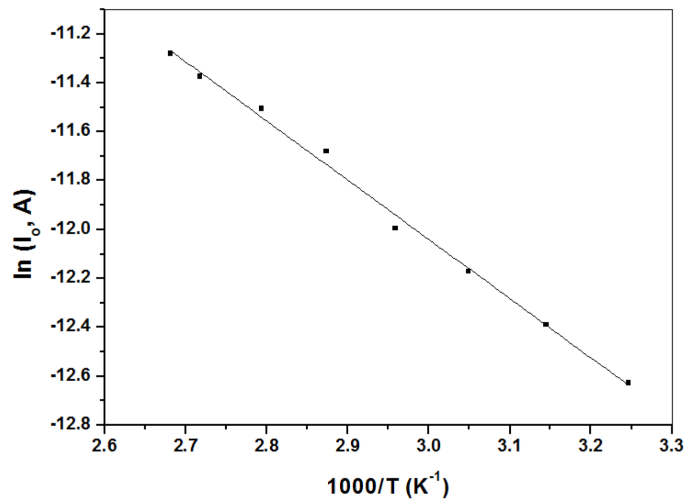

Fig. 5: Temperature dependence of ln I_o for Au/n-$GeSe_4$/p-Si/Al heterojunction.

To compare the values of the barrier heights of the heterojunction with that obtained from the I-V characteristics. Norde (1979) proposed a method based on the following relation (Aksoy *et al.*, 2012)

$$F(V) = \frac{V}{\gamma} - \frac{kT}{q} ln\left(\frac{I(V)}{A^* A T^2}\right) \quad (6)$$

where γ is an integer greater than n, V is the junction applied voltage and $I(V)$ is the corresponding current. The barrier height can be calculated from the relation

$$\Phi_B = F(V_o) + \frac{V_o}{\gamma} - \frac{kT}{q} \tag{7}$$

where $F(V_o)$ is the minimum value of $F(V)$ and V_o is the corresponding voltage. Fig. 6 shows the plot of Norde function $F(V)$ versus V of Au/n-$GeSe_4$/p-Si/Al heterojunction at different temperatures. The calculated values of the barrier height obtained using Norde method are shown in table 1.

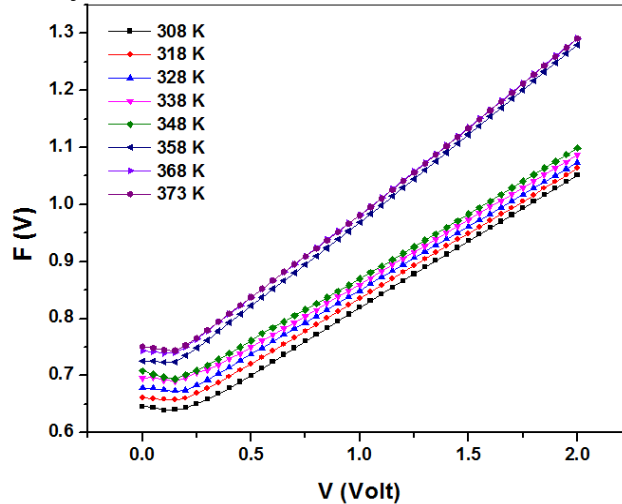

Fig. 6: Plot of $F(V)$ versus V for Au/n-$GeSe_4$/p-Si/Al heterojunction at different temperatures.

The relation between the barrier heights calculated from the I-V characteristics, Norde method and the ideality factor as a function of temperature were plotted in Fig. 7. The barrier heights calculated from Norde method agreed with that calculated from I-V curves. It is clear that the barrier heights and the ideality factors are strongly temperature dependent. As the temperature decreases, the barrier height decreases and the ideality factor increases. This behavior shows the deviation from the ideal TE theory. Most junctions deviate from ideal TE theory. This may be explained with spatially inhomogeneous barrier heights. This was associated with TE with Gaussian distribution of barrier heights (Evans-Freeman *et al.*, 2011).

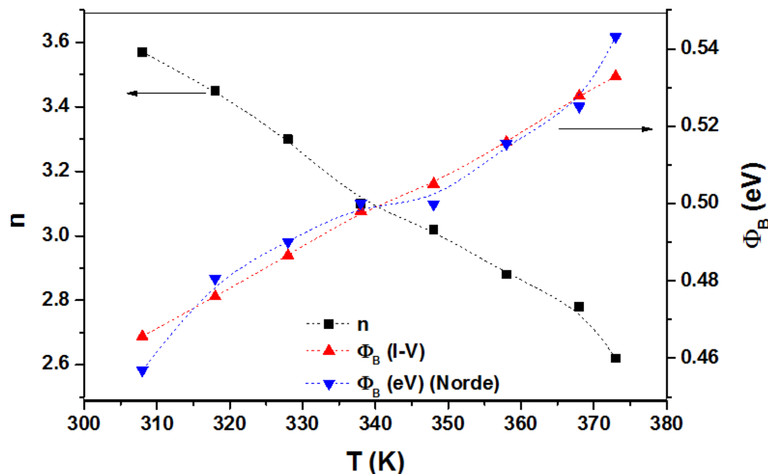

Fig. 7: Temperature dependence of ideality factor n and barrier height Φ_B of Au/n-$GeSe_4$/p-Si/Al heterojunction.

The plot of the zero barrier height versus the ideality factor at each temperature is depicted in Fig. 8. This figure shows that there is an inverse linear relation between Φ_B and n. This relationship can be explained by lateral inhomogenities of the barrier height. The extrapolation of the straight line to n=1 gives the value of homogenous barrier height of 0.652 eV. The barrier heights inhomogeneity for n-$GeSe_4$/p-Si may be due to

lattice constant mismatch and the difference in the thermal expansion coefficients between n-$GeSe_4$ thin films and p-Si (Farag *et al.*, 2009; Roy *et al.*, 2005).

Several authors (Evans-Freeman *et al.*, 2011; Farag *et al.*, 2009; Al-Ktob *et al.* 2013; Janardhanam *et al.*, 2009, 2013; Song *et al.*, 1986) proposed a Gaussian distribution of the inhomogeneous barrier heights with a mean value of barrier height Φ_{Bm} and a standard deviation σ of the barrier height distribution. They proposed that the previously obtained values of barrier height and ideality factor are apparent and denoted by Φ_{ap} and n_{ap}, respectively. The relation between the apparent barrier heights and the mean value of the barrier height is given by the relation (Song *et al.*, 1986; Chand *et al.*, 2005).

$$\Phi_{ap} = \Phi_{Bm} - \frac{q\,\sigma^2}{2kT} \quad (8)$$

The variation of apparent ideality factor with temperature is given as (Werner *et al.*, 1991)

$$\left(\frac{1}{n_{ap}} - 1\right) = -\rho_2 + \frac{q\rho_3}{2kT} \quad (9)$$

where ρ_2 and ρ_3 are the voltage deformation coefficients of the barrier height. Fig. 9 shows the plot of Φ_{ap} and $(\frac{1}{n_{ap}} - 1)$ versus $\frac{q}{2kT}$. Using equation (8) the mean barrier height and the standard deviation can be calculated from the intercept and the slope of the linear fit of the plot. The obtained mean barrier height and the standard deviation were 0.847 and 0.143 eV, respectively. The lower value of σ corresponds to homogeneous barrier height. However, σ = 0.143 eV is high compared to $\Phi_{Bm} = 0.847$ eV (~17% from its value). This confirms the presence of barrier height inhomogeneties. While, the voltage deformation coefficients can be obtained from the intercept and slope of the linear fit of the plot of $\left(\frac{1}{n_{ap}} - 1\right)$versus $\frac{q}{2kT}$ according to equation (9). The ρ_2 and ρ_3 were calculated to be −0.174 and −0.029 mV, respectively. These values are in agreement with the values reported earlier (Janardhanam *et al.*, 2013).

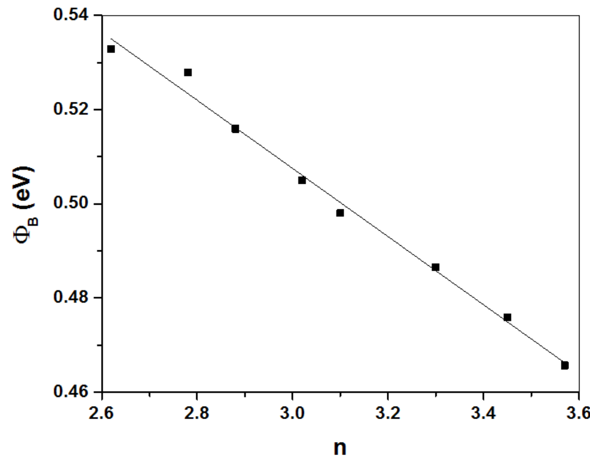

Fig. 8: Plot of barrier height versus ideality factor for Au/n-$GeSe_4$/p-Si/Al heterojunction.

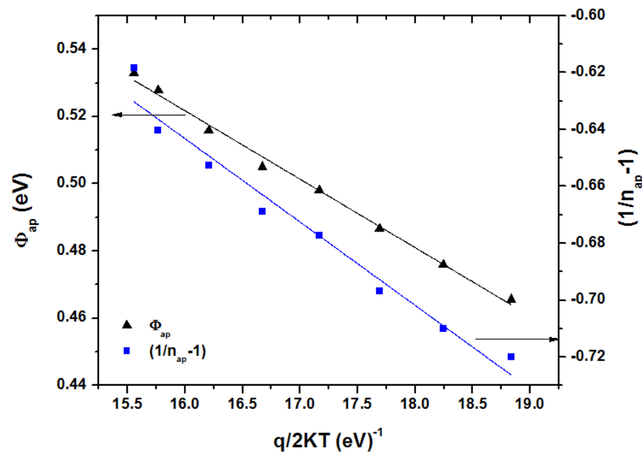

Fig. 9: The barrier height and ideality factor versus *q/2kT* plot of Au/n-$GeSe_4$/p-Si/Al heterojunction.

The measurement of the capacitance-voltage (C-V) study is important to determine valuable electrical parameters of the heterojunction. The carrier concentration, the width of the depletion layer and the flat band potential can be obtained from that study. Fig. 10 shows the dark capacitance-voltage behavior (C^{-2}-V) of Au/n-$GeSe_4$/p-Si/Al heterojunction measured at room temperature at 1 MHz. This high frequency is sufficient to prevent interface states charges to contribute to the capacitance measurement. The capacitance of the junction is given by the relation (Sze, 1981)

$$\frac{1}{C^2} = \frac{-2}{eA^2N\varepsilon\varepsilon_o}\left(V_{bi} - \frac{kT}{q} - V_r\right) \quad (10)$$

where V_{bi} is the built-in voltage which can be obtained from the extrapolation of the linear fit to the voltage axis, V_r is the reverse voltage, *N* is the net carrier concentration, ε is the dielectric constant of $GeSe_4$ ($\varepsilon = 2.45$) (Pan *et al.*, 2009) and A is the effective area. It is clear from the relation (10) that C^{-2} increases linearly with decreasing reverse voltage. This linearity of the plot confirms the formation of abrupt heterojunction. The slope of the linear fit of the figure is given by

$$Slope = \frac{d(C^{-2})}{dV} = -\frac{2}{eA^2N\varepsilon\varepsilon_o} \quad (11)$$

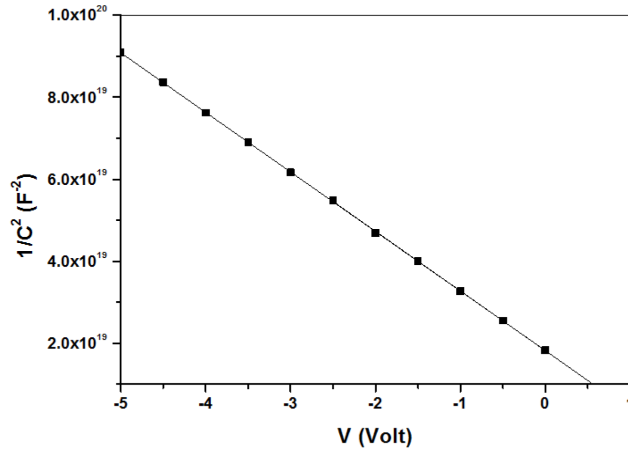

Fig. 10: The variation of C^{-2} versus V for Au/n-$GeSe_4$/p-Si/Al heterojunction.

The x-intercept of the plot gives V_o, which is related to the built-in voltage by the relation ($V_{bi} = V_o + \frac{kT}{q}$). The built-in voltage, the capacitance at zero bias was derived from the figure to be 0.574 V, and 2.33× 10^{-10} F, respectively. The width of the depletion region (*W*) is related to C_o by the relation:

$$W = \frac{\varepsilon\varepsilon_o A}{C_o} \quad (12)$$

And the maximum electric field is related to the depletion region is given by

$$E_{max} = \frac{2V_{bi}}{W} \quad (13)$$

The obtained values of W and E_{max} were calculated to be 0.42 µm and 2.74V/µm, respectively.

Another conduction mechanism is operating in reverse bais. The reverse current resulting from generation recombination of carriers according to the thermally activated relation (Ahmed *et al.*, 2004).

$$I_R = I_{OR} \exp\left(-\frac{\Delta E_t}{kT}\right) \quad (14)$$

where ΔE_t is the thermal activation energy. The relation between *log* I_R versus *1000/T* at different voltage are depicted in Fig.11. The slope of the linear fit gives the thermal activation energy and it is found to vary from 0.21-0.31 eV depending on the applied voltage.

The exponential dependence of reverse current on applied voltage (Fig. 2) suggests Poole-Frenkel or Schottky barrier lowering operating in the depletion region (Simmons, 1971). According to Poole-Frenklel barrier lowering leads to reverse leakage current given as (Simmons, 1971)

$$I = I_o \exp\left(\frac{\beta_{PF}V^{1/2}}{kTd^{1/2}}\right) \quad (15)$$

while Schottky lowering is (Simmons, 1971):

$$I = AA^*T^2 \exp\left(\frac{\beta_S V^{1/2}}{kTd^{1/2}}\right) \quad (16)$$

where β_{PF} and β_S are Poole-Frenkel and Schottky field lowering coefficients. Fig. 12 shows the dependence of the reverse current versus $V^{1/2}$. The obtained straight lines confirmed that the Poole-Frenkel or Schottky

mechanism is dominating. The value of Poole-Frenkel coefficient was calculated and found to be 2.17×10^{-24} $eVm^{1/2}V^{1/2}$.

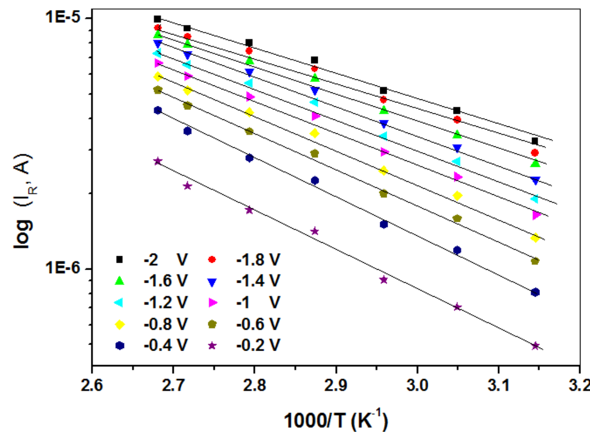

Fig. 11: Temperature dependence of log I_R for Au/n-$GeSe_4$/p-Si/Al heterojunction.

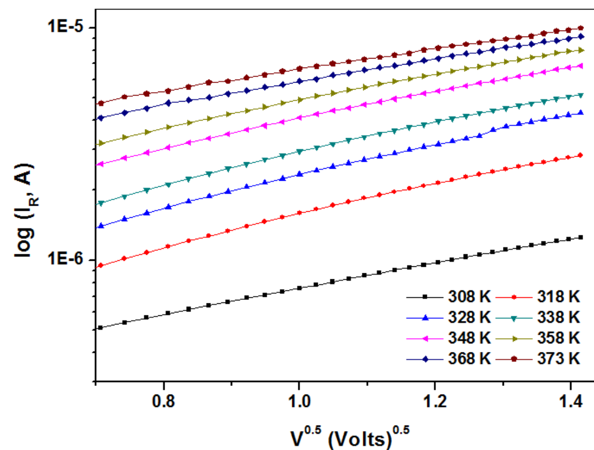

Fig.12: Plot of log I_R versus $V^{0.5}$ for Au/n-$GeSe_4$/p-Si/Al heterojunction.

Conclusion:

Amorphous n-$GeSe_4$ thin films were deposited by thermal deposition technique on p-Si wafer to prepare Au/n-$GeSe_4$/p-Si/Al heterojunction. Investigation of the heterojunction indicated good rectification ratio at ± 1V. The ideality factor and the barrier heights were strongly temperature dependent. At low bias, the thermionic theory was proposed as the predominant transport conduction mechanism. The ideality factor were found to decrease while, the barrier heights increased with increasing temperature. This deviation from the ideal TE theory was explained by the spatially inhomogeneous barrier heights. The extrapolation of the straight line for the dependence between Φ_B and n gives the homogeneous barrier height of 0.652 eV. The mean barrier heights and standard deviation obtained from the Gaussian distribution of inhomogeneous barriers were calculated. While, the voltage deformation coefficients were calculated to be −0.174 and −0.029 mV, respectively. The built-in voltage, the capacitance at zero bias, width of the depletion region was derived from C-V measurements as 0.574 V, 2.33×10^{-10} F, and 0.42 µm, respectively. The reverse biased characteristics were explained in terms of Poole-Frenkel or Schottky effects.

References

Ahmed, M.M., Kh.S. Karimov and S.A. Moiz, 2004. IEEE Trans. Electron. Devices 51: 121-126.
Aksoy, S. and Y. Caglar, 2012. Superlatt. Microstruct., 51: 613-625.
Al-Kotb, M.S., J.Z. Al-Waheidi and M.F. Kotkata, 2013. Super. Microelec., 55: 131-143.
Anderson, R.L., 1962. Solid State Electron., 5: 341-344.
Borrisova, Z.U., 1981. Glasses Semiconductors, Plenum Press, New York.

Capasso, F., G. Margaritodo, 1987. Heterojunction Band Discontinuity Physics and Devices Applications, North-Holland, Amsterdam.
Çetinkara, H.A., A. Türüt, D.M. Zengìn and Ş. Erel, 2003. Appl. Sur. Sci., 207: 190-199.
Chand, S. and S. Bala, 2005. Appl. Sur. Sci., 252: 358-363.
El-Nahass, M.M., E.F.M. El-Zaidia, M.H. Ali and I.T. Zedan, 2014. Mater. Sci. Semicond. Process, 24: 254-259.
El-Nahass, M.M., I.T. Zedan and A.A. Atta, 2012. Eur. Phys. J. Appl. Phys., 59: 20101-1-6.
Evans-Freeman, J.H., M.M. El-Nahass, A.A.M. Farag and A. Elhaji, 2011. Microelect. Eng., 88: 3353-3359.
Farag, A.A.M., F.S. Terra, G.M. Mahmoud and A. M. Mansour, 2009. J. Alloys Comp., 481: 427-433.
Hafiz, M.M., A.A. Othman, M.M. El-Nahass and A.T. Al-Moatasem, 2007. Physica B, 390: 348-355.
Hamakawa, Y., (ed.), 1981. Amorphous Semiconductor; Technology and Devices, Ohm & North-Holland, Amsterdam.
Hor, A.M. and R.O. Loutfy, 1983. Thin Solid Films, 106: 291-301.
Janardhanam, V., A.A. Kumar, V.R. Reddy and P. N. Reddy, 2009. J Alloys Comp., 485: 467-472.
Janardhanam, V., I. Jyothi, K.S. Ahn and C.J. Choi, 2013. Thin Solid Films, 546: 63-68.
Kokorina, V.F., 1996. Glasses for Infrared Optics, CRC Press, Boca Raton.
Lee, W-Jae, J. Sharp, G.A. Umana-Membreno, J. Dell and L. Faraone. 2015. Materials Sci. Processing, 30: 413-419.
Norde, H., 1979. J. Appl. Phys., 50: 5052-5053.
Pan P.K., H.Z. Zang, X.J. Zhao, T.J. Zhang, 2009. J. Alloys Comp., 484: 645-648.
Pan, R.K., H.Z. Tao, J.Z. Wang, J.Y. Wang, H.F. Chu, T. J. Zhang, D.F. Wang and X.J. Zhao, 2013. Optik, 124: 4943-4946.
Popescu, M.A., 2000. Non-Crystalline Chalcogenides, Kluwer Academic Publishers, Dordrecht.
Roy, S., C. Jacob and S. Basu, 2004. Solid State Sci., 6: 377-382.
Russo, L., M. Vlecek and H. Jain, 2005. Glass Technol., 46: 94-98.
Sedeek, K., A. Adam, M.R. Balboul, L.A. Wahab and N. Makram, 2008. Mater. Res. Bull., 43: 1355-1362.
Simmons, J.S., 1971. J. Phys., D4: 613-657.
Song, Y.P., R.L. Van Meirhaeghe, W.H. Laflere and F. Cardon, 1986. Solid State Electron., 29: 633-638.
Sze, S.M., 1981. Physics of Semiconductor Devices, New York, Wiley.
Thakur, A., G. Singh, G.S.S. Saini, N. Goyal and S.K. Tripathi, 2007. Opt. Mater., 30: 565-570.
Tikhomirov, V.K., A.B. Seddon, K. Asatryan, T.V. Galstian and R. Vallee, 2003. J. Non-Crystall. Solids, 326-327: 205-208.
Troles, T., V. Shiryaev, M. Churbanov, P. Houizot, L. Brilland, F. Desevedavy, F. Chrpentier, T. Pain, G. Snopatin and J.L. Adam, 2009. Optical Mater., 32: 212-215.
Tucci, M., L. Serenelli, E. Salza, M. Ratté, S. De Luliis, L.J. Geerligs, D. Caputo, A. Nascetti and G. de Cesare, 2007. Thin Solid Films, 516: 6771-6774.
Werner, J.H. and H.H. Güttler, 1991. J. Appl. Phys., 69: 1522-1533.
Zhang, Y., J. Xu, B. Lin, Z. Fu, S. Liu and S. Zhong, C. Liu and Z. Zhang, 2006. Appl. Sur. Sci., 252: 3449-3453.